Universal Sources of Accelerated Particles and Metal Vapor for Industrial-Scale Beam-Assisted Deposition

S.N. Grigoriev, A.N. Isaikov, Yu.A. Melnik, A.S. Metel

State University of Technology STANKIN, Vadkovsky per. 1, Moscow, 127055, Russia,
Phone: 095-973-3103, Fax: 095-973-3866, E-mail: sgrigor@stankin.ru

Abstract – A beam-assisted deposition technique is presented featuring a fast neutral molecule beam combined with a metal vapor flow from one and the same emissive grid being used instead of vapor flows and ion beams from separate sources. Immersion inside the plasma emitter of a target turns fast neutral molecule beam sources into universal sources of ~ 10-kVA broad electron beams for preheating of massive substrates, of ~ 1-keV neutral molecules for pre-cleaning of the substrate surface, as well as of metal vapor to be deposited on the substrate the deposition being assisted with ~ 100-eV molecules. Tests of a universal source with a 16-cm-diam disc-shaped Ti-target and 22-cm-diam flat grid showed a homogeneous sputtering of the whole 200 cm^2 target area with 1–3 keV argon ions at the ion current density up to 20 mA/cm^2. The source may allow homogeneous TiN-film deposition rate up to 7 μm/h on 20-cm-diam substrates.

1. Introduction

Important properties of thin films deposited by means of material vaporization in vacuum, such as structure, density, hardness and internal stress, are influenced by ions bombarding the films during deposition. For a beam-assisted deposition on conductive substrates it is enough to immerse them in plasma, which contains all needed components ionized, and to apply to them an optimum negative bias voltage. This method is widely used in many industrial vacuum deposition systems. Among its disadvantages a high heterogeneity of ion current density over the surface of any complex-shaped substrate. The current density is many times higher at the substrate sharp edges than in the slots. And it often leads to blunting of the tool cutting edges.

The bias voltage cannot be applied to dielectric substrates and films. In this case broad-beam sources are indispensable for the beam-assisted deposition. As the bias power supply current of industrial systems in many cases reaches 10 A and more, the beam current should also reach at least the same value at any energy ranging from 10 eV to 1 keV to ensure characteristics optimization of deposited films.

The broad-beam method may be applied to any materials. In addition, it can ensure homogeneous treatment of sharp edges and slots. The only obstacle for substitution of the bias voltage method with the more universal broad-beam method in all industrial systems is a lack of adequate beam sources in the world market.

The problem was solved after development of fast neutral molecule beam sources [1, 2]. The fast molecules are being produced [2] as a result of charge exchange collisions between accelerated ions and slow molecules near the emissive grid of the beam source. The ion acceleration-deceleration in two space charge sheaths separated from each other with one grid allows beam current density up to 10 mA/cm^2 at any energy of accelerated particles beginning from 10 eV up to several keV. The sources offer the beam cross-section up to 10^4 cm^2, equivalent beam current up to 10 A and lead to industrial-scale beam-assisted deposition at 0.05–0.6 Pa. As compared with ions the fast neutral molecules ensure better treatment stability, reliability, eliminate damage of conductive films with sparks and reduce the number of defects, which are induced with charged particles in dielectrics and semiconductors.

2. Basic Principles of Combined Beam Production

Figure 1 schematically presents a system equipped with a universal source, which comprises a cylindrical grid 1, a cathode 2, an anode 3 and a coaxial with the grid 1 water-cooled tube-shaped target 4, which may be negatively biased in respect to the cathode 2 using a DC power supply 5. At zero bias voltage, the target 4 is equipotential with the cathode 2 and both are parts of an electrostatic trap, which confines electrons. A DC power supply 6 keeps the grid 1 negative to the cathode 2, thus preventing the electrons emitted with the cathode 2 from leaving the trap through the holes of the grid 1. At a discharge voltage of several hundred V from a DC power supply 7, a high-current beam of accelerated ions extracted from a plasma emitter 8 enters the working chamber 9, turns into a neutral molecule beam and treats the substrates 10 positioned all around the beam source on the substrate rotating system 11. The beam energy corresponds to output voltage of DC power supply 12 and may be regulated from zero to several keV. Beam particles, which pass through the gaps between the substrates 10, are absorbed with a jalousie-type set of plates 13, the incident angle of beam particles to the plates 13 exceeding 70°. It is needed to prevent from sputtering of the plates and from deposition of their material on the other sides of the substrates.

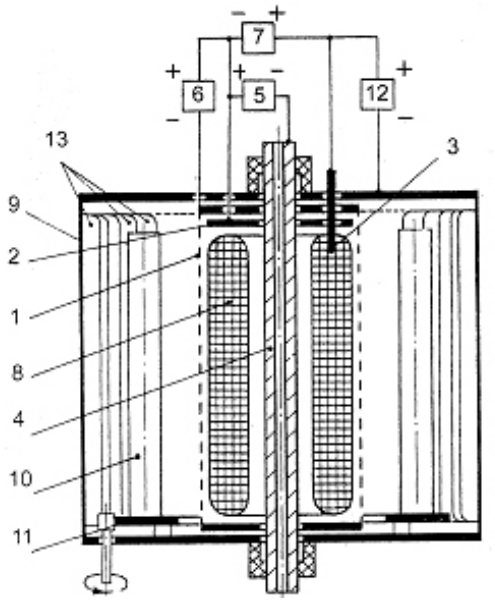

Fig. 1. Schematic diagram of a system equipped with a universal beam source: 1 – cylindrical grid; 2 – cathode; 3 – anode; 4 – target; 5, 6 – bias-voltage power supplies; 7 – discharge power supply; 8 – plasma emitter; 9 – vacuum chamber; 10 – substrates; 11 – substrate rotating system; 12 – accelerating voltage power supply; 13 – jalousie-type set of beam absorbing plates

At zero bias voltage of power supply 5, the system may be used for etching the substrates with 500–1000 eV molecules. If bias voltage of 10–15 kV is applied, the target 4 may be used as a source of ~ 10 kVA beam of electrons heating the substrates. At a bias voltage of 1–3 kV and ion current of 2–10 A in the target circuit, the target 4 turns into an intensive source of the target material vapor. The vapor reaches the substrates 10 through the high-transparency grid 1 and deposition of the vapor may be assisted with a beam of low-energy molecules. Variation of power supplies` parameters allows a wide-range regulation of beam energy E and of flow densities ratio B/V of beam and vapor particles, which follow one and the same way from the grid to the substrate surface. It allows a wide-range regulation of film characteristics.

3. Experimental Set-up

To choose optimum sizes of the system, gas pressure and parameters of all power supplies presented in Fig. 1 it is needed first to investigate the simplest model of a universal source with circular cross-section of the beam. Fig. 2 presents an experimental source, which comprises four main parts: a cylindrical 30-cm-diam to 10-cm-long hollow cathode 1, an anode 2, a 22-cm-diam emissive grid 3 and a 16-cm-diam water-cooled target 4, all of them mounted inside a water-cooled cylindrical 36-cm-diam to 23-cm-long case 5. The grid is produced of a 0.8-mm-thick titanium sheet. The distance between the centers of neighboring each other 4.6-mm-diam holes of the grid is equal to 5 mm and the grid transparency amounts to 77%.

As the total current in the anode circuit of the beam source should exceed 20 A, the DC power supplies presented in Fig. 1 should be arc-handling. It was decided to use first for investigation of the *V-A* characteristics a cheaper method of power supply with sinusoidal 100-Hz pulses, based on two 220/380V-transformers 6, 7 and one 220/3000V-transformer 8 (Fig. 2). When only the transformer 6 is switched on positive in respect to the grid 3 and to the grounded case 5 voltage pulses of 540 V amplitude from the bridge-rectifier 9 are being applied to the anode 2. When the transformers 6 and 7 are simultaneously switched on the total amplitude of pulses applied to the anode from the rectifiers 9 and 10 amounts to 1080 V. Negative in respect to the cathode 1 pulses of 4.2-kV amplitude are being applied to the target 4 from the rectifier 11 after the transformer 8 is switched on.

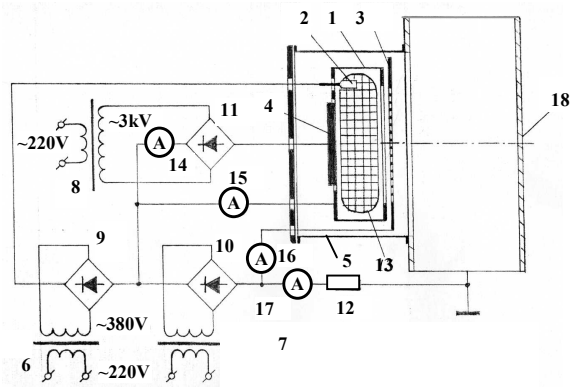

Fig. 2. Schematic diagram of the universal source: 1 – hollow cathode; 2 – anode; 3 – grid; 4 – target; 5 – case; 6–8 – transformers; 9–11 – rectifiers; 12 – resistor; 13 – plasma emitter; 14–17 – ammeters; 18 – chamber

Pulsed current through the resistor 12 [1] with a variable up to 250 O resistance induces negative voltage pulses applied to the grid 3, which limit the current of electrons penetrating through the grid 3 into the plasma emitter 13. Effective mean currents in the circuits of the target 4, cathode 1, grid 3 and chamber 18 were measured with the DC ammeters 14–17. Waveforms of currents in the circuits of the target 4 and of the cathode 1 were registered with Rogovsky coils and in the circuit of the chamber – with a low-inductance shunt. Voltage pulses applied to the anode 2 and to the target 4 were registered in respect to the ground potential.

Gas pressure was measured with a plasma-shielded ion gage PMI-2 positioned in another 0.1 m^3 chamber with no gas flowing through it, which communicated with the working chamber.

To ensure at the gas pressure $p \sim 0.1$ Pa a reliable ignition of the glow discharge inside the beam source the chamber 18 and the hollow cathode 1 of the beam source were being filled with the ion-producing gas through a pre-ionization arrangement mounted on the chamber wall. Due to 50-mA DC glow discharge in

the arrangement a low-density plasma continuously filled the chamber 18 and the hollow cathode 1 when the beam source was out of operation. At the top of the chamber 18 a Langmuir probe was mounted in order to measure the plasma potential φ inside the chamber.

4. Investigation of Discharge Parameters

The first experiments revealed dependence of the low-pressure limit for the discharge ignition on the form and position of the anode 2. When it is shaped as a 4-cm-long tuning fork, positioned near the cathode surface and distanced at 11 cm from the axis of the cathode the discharge may be ignited only at $p > 0.8$ Pa. The reason is that at lower pressure the plasma density is rising slower than the cathode sheath width, the anode finds itself in the sheath and it hinders the discharge. The problem was solved after another L-shaped anode made of 4-mm-diam to 25-cm-long steel rod was used, which crossed the axis of the cathode 1 and was equidistant from the grid 3 and the target 4. As a result the pressure limit diminished down to 0.1 Pa.

Another problem caused by the beam divergence was overheating of the chamber's fitting flange (not shown in Fig. 2). To solve this problem the flat grid was replaced with a spherical grid of ~ 20-cm radius. A modernized model of the source is shown in Fig. 3.

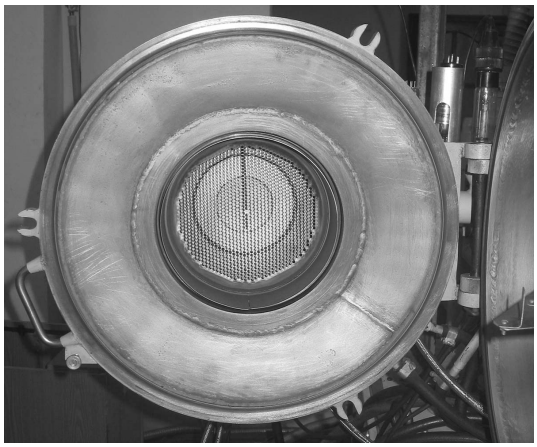

Fig. 3. Photograph of the source with two (Ti and Al) targets, rod-shaped anode, and spherical emissive grid

When transformer 6 was switched on sinusoidal pulses of the anode potential U presented in Fig. 4,a with a chain curve heightened the low-density plasma potential inside the hollow cathode 1 and at $U > 200$ V it resulted in a self-sustained discharge. The hatch curve 1 in Fig. 4,b presents a waveform of the cathode current at argon pressure $p = 0.2$ Pa and 20-O resistance of the resistor 12. The hatch curves 2 and 3 in Fig. 4,b present current waveforms in the circuits, respectively, of the chamber and of the aluminum target. All the currents reach maximum values in 6.5 ms after zero voltage point: 9 A in the cathode, 5.5 A in the chamber and 2 A in the target circuits.

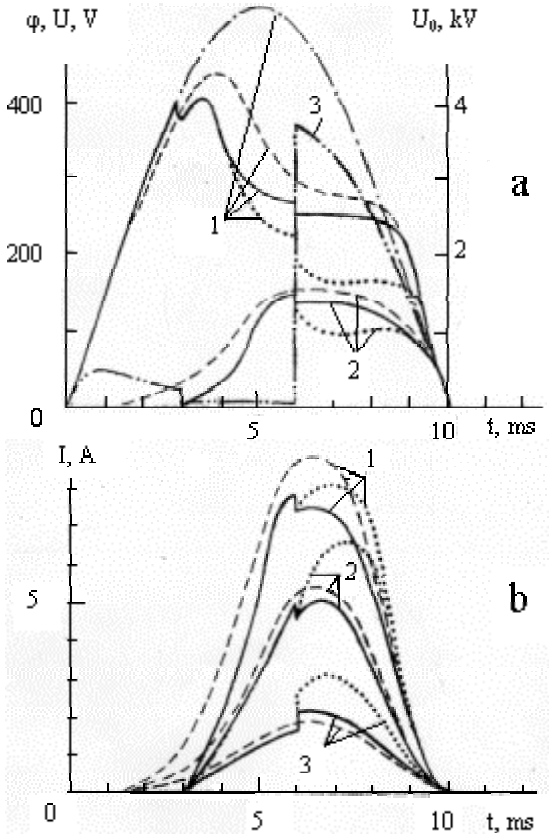

Fig. 4. a – waveforms of the anode potential U (1), chain curve presents the U waveform at zero currents, of the plasma potential φ in the chamber (2) and of the target potential U_0 (3); b – current waveforms in the circuits of the cathode (1), of the chamber (2) and of the target (3) at $p = 0.2$ Pa of argon at $U_0 = 0$ (hatch curves), of argon at $U_0 \neq 0$ (full curves) and of argon (80%) to nitrogen (20%) mixture at $U_0 \neq 0$ (dashed curves)

Taking into account the current of 3.5 A in the grid circuit the total current amplitude in the anode circuit amounts to 20 A. Such current through transformer 6 results in a distortion of the sinusoidal voltage. In addition the anode potential is diminished due to the voltage drop through the resistor 12. As a result U waveform presented in Fig. 4,a with a hatch curve 1 is highly distorted and at the maximum current the anode potential amounts to 275 V.

The hatch curve 2 in Fig. 4,a presents a waveform of plasma potential φ inside the chamber 12, which reaches its maximum value of 150 V at the maximum current. So, high plasma potential is the result of an inadequate space charge compensation of ions injected from the source with secondary electrons from the grid and the chamber walls. The reason is a drain of the electrons through the grid holes to the plasma emitter. A resistance increase up to 100–200 O of the resistor 12 stops the electron drain and leads to a decrease of the φ down to 10 V. However, it also leads to a decrease of the discharge current because even a small current of electrons injected from the chamber into the hollow cathode of the beam source increases the gas ionization rate in the cathode [1].

Energy of accelerated argon ions corresponds to the potential difference between the plasma emitter 13 and the plasma inside the chamber. In the case under consideration it amounts to 275 V – 150 V = 125 V. Due to charge exchange collisions the ions turn into 125-eV neutral molecules bombarding the substrates distanced at ~ 20 cm from the grid. The amplitude of their equivalent current amounts to ~ 4 A.

When the transformers 6, 8 (Fig. 2) are switched on simultaneously high energy of ions bombarding the target 4 leads to intensive sputtering of the target material, which is partially deposited on the hollow cathode 1. For this reason it does not matter what was the initial material of the cathode. In fact it was made of steel, but after 15-min sputtering of the titanium target the cathode should be considered as made of titanium from the point of view of the discharge characteristics. After the titanium target is replaced with the aluminum one it should be considered as made of aluminum and so on.

The first switching on of the transformer 8 led at the argon pressure of 0.2 Pa to extinguishing of the discharge. The reason was the same: a high widening rate of the sheath near the target, which covered the rod anode before the plasma density could reach a safe level. The problem was solved by means of a thyristor switch, which allowed a delay variation of the high voltage application to the target after the zero-voltage point. The curve 3 in Fig. 4,a presents a waveform of the negative target potential U_0, which may be divided in three intervals: a low-voltage one within the first 3 ms, a zero-voltage one within the following 3 ms and a high-voltage interval within the last 4 ms till the next zero-voltage point. The potential difference between the anode and the target is equal to the sum of U and U_0 and reaches in the first interval its maximum of ~ 500 V much earlier than the anode potential U reaches the same value and this hinders the discharge ignition.

As soon as U_0 drops down to zero the sum $U + U_0$ from 700 V drops down to 400 V, the width of the target sheath diminishes, the rod anode finds itself in the plasma and it leads to ignition of the discharge. The full curves of the Fig. 4,b present the current waveforms in the circuits of the cathode (1), chamber (2) and of the target (3). The currents are rising faster than without switching on the transformer 8 and just before the high-voltage interval they reach about the same values. When the negative potential of the target reaches 3.7 kV a 0,4-A-high step of the target current waveform appears, which gives information on the current of 4-keV secondary electrons emitted by the target. The electrons reach the grid and about 77% of them through the grid holes enter the chamber. At this moment the electron current amounts to ~ 20% of the ion current. The electron beam leads to appearance of the steps at all other waveforms indicating a small decrease in the cathode and chamber currents as well as in the anode and plasma potentials.

At the same pressure p = 0.2 Pa of argon-nitrogen mixture (80% and 20%, respectively) the waveform step of the target current amounts to ~ 0.75 A. It means that interaction of nitrogen with the aluminum target results in about twofold increase of secondary electron emission. All the waveforms related to the addition of nitrogen are presented in Fig. 4 with dashed curves. Higher electron beam current results in a substantial increase of all the currents and in a decrease of the anode potential U down to 170 V and of the plasma potential φ down to 100 V. It means that in this case film deposition on dielectric substrates positioned inside the chamber is assisted with 70-eV argon and nitrogen molecules.

5. Film Deposition

The above universal beam source allowed deposition of TiN, AlN and TiAlN films using an argon-nitrogen mixture and of metallic films using a pure argon. To deposit TiAlN films two targets were used: an inner aluminum 90-mm-diam disc and an outer titanium 90/160-mm-diam annular target. The films practically had no droplets because glow-to-arc transitions were very seldom due to pulsed regime of power supply. To ensure an adequate adhesion of the films the substrates before deposition were pre-cleaned with 700–900 eV argon atoms within ~ 10 minutes. For pre-cleaning only transformers 6 and 7 (Fig. 2) should be switched on.

In the case characterized in Fig. 4 with full curves the deposition rate of Al films on glass substrates depended on distance l from the emissive grid of the source amounting to 3 μm/h at l = 7 cm, to 1.5 μm/h at l = 21 cm and to 1.0 μm/h at l = 35 cm. The waveforms show that the deposition takes less than 4 ms of each 10-ms-wide pulse period. If the DC arc-handling power supplies could be used, which keep constant all currents and potentials established just after application to the target of the high voltage at t = 6 ms the amount of Al atoms deposited during 2 ms would be approximately equal to the total amount of atoms deposited during our 10-ms-wide pulse period. It means that in the DC regime the universal beam source could ensure about 5 times higher deposition rate of Al films amounting to ~ 10 μm/h.

When the Al target is replaced with a Ti target at the same argon pressure and in the same power supply regime the deposition rate decreases 1.5–2 times due to lower sputtering yield for titanium. Using the mixture of argon (80%) and nitrogen (20%) 2.8-μm-thick TiN films with 2300HV_{50} microhardness have been deposited during 2 hours on tungsten carbide samples distant at 20 cm from the source grid. The above estimates allow suggestion that using DC arc-handling power supplies the source could allow TiN deposition rate of 7 μm/h.

In the $Ar–N_2$ mixture with Al target black dielectric AlN films have been deposited on conductive

and dielectric substrates. It turned out that properties of AlN films depend on the distance l from the grid. At $l = 21$ cm the film is quite homogeneous and dielectric, but at $l = 7$ cm the beam electrons print on a substrate made of glass a projection of the grid with its holes marked as defected and conductive circular areas of the film.

6. Conclusions

The above results demonstrate abilities of new devices for beam-assisted deposition. One and the same device produces broad electron beam for heating the substrate in vacuum, metal vapor to be deposited and broad beam of fast molecules for pre-cleaning the substrate surface and for modification of the film during the deposition.

The obtained data show the way to industrial film deposition without droplets and other serious defects with a rate of ~ 10 μm/h. Deposition of conductive or dielectric films is available on conductive as well as dielectric substrates.

The beam of secondary electrons is an effective means for heating of massive substrates before the film deposition. But it seems to play no positive role during the deposition. As the electron emission rises when reactive gases (N_2, O_2 and others) are added to the target sputtering gas (Ar, Kr) an attempt should be made to independently fill the beam source with inert gas and to add the reactive gas in the close vicinity of the substrate surface in the working chamber.

References

[1] A. Metel, S. Grigoriev, *US Patent 6,285,025*, 2001.

[2] S. Grigoriev, Yu. Melnik, A. Metel, Surface and Coating Technology **156**, 44 (2002).